Journal of Biomedical Optics

BiomedicalOptics.SPIEDigitalLibrary.org

Bioluminescence of *Vibrio fischeri*: bacteria respond quickly and sensitively to pulsed microwave electric (but not magnetic) fields

Catrin F. Williams
Gilles M. Geroni
David Lloyd
Heungjae Choi
Nicholas Clark
Antoine Pirog
Jonathan Lees
Adrian Porch

Catrin F. Williams, Gilles M. Geroni, David Lloyd, Heungjae Choi, Nicholas Clark, Antoine Pirog, Jonathan Lees, Adrian Porch, "Bioluminescence of *Vibrio fischeri*: bacteria respond quickly and sensitively to pulsed microwave electric (but not magnetic) fields," *J. Biomed. Opt.* **24**(5), 051412 (2019), doi: 10.1117/1.JBO.24.5.051412.

Journal of Biomedical Optics 24(5), 051412 (May 2019)

Bioluminescence of *Vibrio fischeri*: bacteria respond quickly and sensitively to pulsed microwave electric (but not magnetic) fields

Catrin F. Williams,[a,*] Gilles M. Geroni,[a] David Lloyd,[b] Heungjae Choi,[a] Nicholas Clark,[a] Antoine Pirog,[a] Jonathan Lees,[a] and Adrian Porch[a]
[a]Cardiff University, School of Engineering, Cardiff, Wales, United Kingdom
[b]Cardiff University, School of Biosciences, Cardiff, Wales, United Kingdom

Abstract. Biological systems with intrinsic luminescent properties serve as powerful and noninvasive bioreporters for real-time and label-free monitoring of cell physiology. This study employs the bioluminescent marine bacterium *Vibrio fischeri* to investigate the effects of separated microwave electric (E) and magnetic (H) fields. Using a cylindrical TM_{010} mode aluminum resonant cavity, designed to spatially separate E and H fields of a pulsed microwave (2.45 GHz) input, we sampled at 100-ms intervals the 490-nm emission of bioluminescence from suspensions of the *V. fischeri*. E-field exposure (at 4.24 and 13.4 kV/m) results in rapid and sensitive responses to 100-ms pulses. H-field excitation elicits no measurable responses, even at 100-fold higher power input levels (equivalent to 183 A/m). The observed effects on bacterial light output partially correlate with measured E-field-induced temperature increases. In conclusion, the endogenous bioluminescence of *V. fischeri* provides a sensitive and noninvasive method to assess the biological effects of microwave fields.
 [DOI: 10.1117/1.JBO.24.5.051412]

Keywords: noninvasive; bioreporter; electromagnetic; thermal; nonthermal.

Paper 180520SSRR received Aug. 29, 2018; accepted for publication Jan. 21, 2019; published online Feb. 28, 2019.

1 Introduction

We live in a fast-growing world of connected information technology that is represented by concepts such as 5G wireless communication, Internet of Things, as well as connected cars and healthcare. These technologies utilize a wide range of frequencies which encompass radio frequency, microwave, and millimeter wave bands. Concerns about the possible biological effects of microwave and millimeter wave frequencies on living organisms including humans, and their cellular, tissue, and organ functions persist, despite extensive investigations carried out for over 40 years.[1–4] Published surveys of large human populations, although mainly concluding that effects are minimal,[5] do not entirely dispel the need for cautious controls, e.g., on the use of mobile phones by children.[6]

It is well-established that microwave irradiation accelerates and enhances chemical[7] and enzymatic[8] reaction rates over and above those produced by conventional thermal sources. Similarly, effects on the membranes[9] of and gene expression in bacteria,[10] human cells,[11,12] tissues,[13,14] and human health[15,16] beg the question of whether nonthermal contributions may be responsible.[17] Many of these experiments have used an incident power of $<10\ \mathrm{mW\,cm^{-2}}$, the recommended threshold for safe exposure to microwaves. Some reports indicate nonlinear power and frequency dependencies that are not consistent with heating effects, but which are ascribed to the "complex behavior of the living state.[18–20]" Many theoretical nonthermal models include the Fröhlich condensate[21,22] and the Davydov soliton,[23] but these are still not experimentally validated in biological systems despite an extensive literature. Should the characterization of a nonthermal component of microwave effects be discovered in biology, it would have highly significant importance for microwave exposure limits, as current guidelines are based on thermal measurements only.[24]

Microorganisms serve as convenient systems for study, as, apart from their intrinsic importance in every aspect of human disease and environmental health, they are easily grown, quantified, and many aspects of their genetics, biochemistry, and biology are more easily elucidated in "model" organisms.[25] Microbial systems with endogenous luminescent properties serve as powerful and noninvasive bioreporters for real-time and label-free monitoring of cell physiology. In this study, we use the marine bacterium, *Vibrio fischeri*, as, in addition to these advantageous characteristics, it produces an intense photoemission with a maximum intensity at 490 nm (blue-green light). The bioluminescence is well-studied at the molecular level and the mechanism of photon emission is understood at the biochemical level[26] even if the detailed excited state transitions are still incompletely characterized.[27] Perturbation of the bioluminescence is produced by physical means (e.g., temperature and pressure changes), or by a wide variety of chemical toxicants (e.g., inhibitors of electron transport or biological energy transduction, detergents, anesthetics, and other membrane disruptants).[28]

In this study, we provide details of an *in vitro* experimental set-up for real-time monitoring of *V. fischeri* bioluminescence during microwave irradiation whereby the electric field (E field) and magnetic field (H field) are separated in a TM_{010} mode resonant cavity. Microwave resonant cavities are powerful tools, which enable effective spatial separation of electric and magnetic components of the applied electromagnetic field.

*Address all correspondence to Catrin F. Williams, E-mail: williamscf@cardiff.ac.uk

Resonant cavities can be designed to operate at any microwave frequency by a suitable choice of cavity dimensions, e.g., the radius and length of a cylinder. For the cylindrical cavity mode chosen here (TM_{010}), the resonant frequency is simply inversely proportional to the radius. Separation of the E and H fields is achieved via the initiation of a standing wave, whereby the E field is maximal in the center of the cavity (axially) and the H field is maximal around the perimeter (circumferentially). This opens the door to many applications, as well as testing fundamental interactions between microwave fields and biological systems.[29] A cylindrical 2.45-GHz resonant cavity operating in its TM_{010} mode has been heavily used for these purposes.[30,31] Not only does this frequency fall within the industrial, scientific, and medical band, and thus used routinely in communications devices, therapeutics, and conventional microwave ovens, its wavelength of ca. 12 cm facilitates a convenient cavity size. Any given resonant cavity can operate at several different modes. We chose the TM_{010} since it is nondegenerate with other modes and has well-defined regions of uniform E field (along its axis) and H field (near its perimeter). By a selecting a suitable choice of radius:length ratio, it can be well-separated from all other modes and so provides a simple microwave excitation system, commonly used to characterize or heat material samples.[32,33]

In this study, we define the E- and H-field distributions within a TM_{010} mode resonant cavity at 2.45 GHz, and their separate effects at various power levels and duty cycles (i.e., pulsing schemes) on the bioluminescence of *V. fischeri*. Our experiments show that although bacterial light emission responds quickly and sensitively to pulsed E fields, at close to nonthermal levels, no effects of exposure to H fields could be demonstrated.

2 Materials and Methods

2.1 *Organism and Culture*

The bioluminescent bacterium employed was *Vibrio fischeri* NRRL-B-11177, kindly supplied by Dr. Michael H. Rayner-Brandes.[34] It was cultured at 25°C on agar containing (in g/l): NaCl (Sigma) 30, peptone (Oxoid) 5, meat extract (Oxoid) 3, $CaCO_3$ 5, agar 15, and glycerol 5 ml.[33] After 24-h growth, organisms were washed off the surface of this growth medium using a buffer containing (g/l) NaCl 23, Na_2HPO_4 15.5, nutrient broth (Oxoid) 10, NaH_2PO_4 2, and glycerol 10 ml. Flasks were plugged with cotton wool for aeration and incubated at 24°C overnight for 20 to 24 h. The organisms were then harvested by centrifugation at 3000 rev/min for 10 min using a benchtop centrifuge (MSE Centaur 11). The sedimented bacteria were washed twice using artificial seawater buffer containing (g/l) NaCl 28.0, $MgCl_2 \cdot 6H_2O$, 5.0, $MgSO_4 \cdot 7H_2O$ 4.5, $CaCl_2 \cdot 2H_2O$ 1.5, and KCl 0.8,[35] and the same centrifugal procedure. They were finally resuspended in artificial seawater for experiments to a density of $\sim 1 \times 10^8$ cells/ml. The artificial seawater provides adequate buffering of the cell suspension, ensuring sustained viability, but starves the cells of nutrients. This eliminates any possible increase in light output associated with cell division, which is not permitted under these conditions.

2.2 *TM_{010} Mode Cavity Resonator*

The cylindrical resonant cavity used was designed and constructed in-house at Cardiff University's Centre for High Frequency Engineering from a solid block of aluminum. This block splits into two halves forming a cylindrical cavity of inner radius 46 mm [Fig. 1(a)]. The specific dimensions of this flattened cylindrical device were designed to achieve resonance at 2.45 GHz with a standing wave such that the maximum electric field occurs down its axis and maximum magnetic field at its circumference when resonating in the TM_{010} mode [Fig. 1(b)]. The resonant frequency of the TM_{010} mode is independent of cavity length, but the inner length was chosen to be 40 mm to ensure good spectral separation of the TM_{010} mode from all other modes (e.g., TE_{111}) while maintaining a high-quality factor Q. This cavity design presents an easily accessed central through-route down its central axis allowing catheter tubing to be inserted vertically, where the E field is at its maximum [Fig. 1(b)]. In the circumferential configuration for H-field

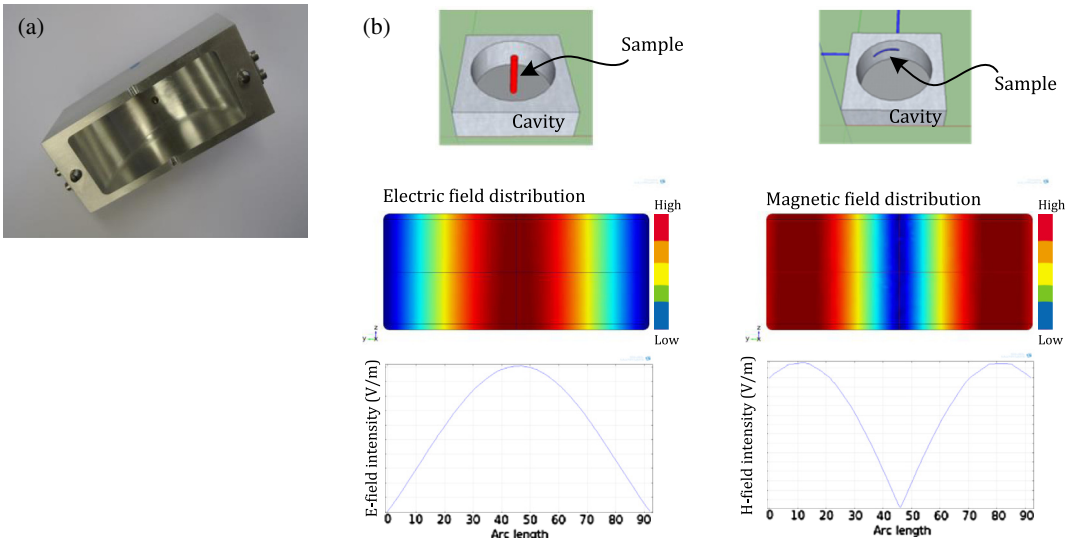

Fig. 1 (a) Inside view of the TM_{010} mode aluminum resonant cavity. (b) Three-dimensional representation of the electric (E) and magnetic (H) field set up, with sample tube placed axially or circumferentially, respectively. E- and H-field intensity plots are also shown.

exposure [Fig. 1(b)], the tube was held in place by thin strips of double-sided adhesive tape. The tape thickness is very thin (~100 μm) and was fixed on the outer metal wall, at which point the electric field is reduced to zero. Measurement of the Q factor and resonant frequency with and without the tube and its fixing, which show negligible differences, indicate that the tape has no impact on the E or H field in this position. To allow for the same sample volume (47.4 μl) for both E- and H-field exposures, an arc length of 50 deg was used for the H-field exposure, meaning that the total length of exposed sample in both cases was 40 mm. Although the heat sinking arrangements are different for the axial and circumferential samples, this is of no issue for comparison between the axial and circumferential experiments since in the former arrangement there is negligible sample heating.

2.3 *Microwave Hardware and Measurements*

The main components of the circuit (Fig. 2) were as follows: (1) microwave signal generator (Telemakus TEG2700-6), which provides a single-tone output at a power level of 6 dBm (i.e., 4 mW rms); (2) microwave switch (Telemakus TES6000-30), which in the "on" position directs the signal to the input of the microwave power amplifier for cavity excitation and into a 50-Ω matched load in the "off" position; (3) microwave power amplifier (Mini-circuits ZHL-30W-262) able to deliver a maximum output power of up to 45 dBm (31.6 W rms) and a linear gain of 50 dB; (4) variable attenuator with 30-dB dynamic range; (5) directional coupler (Mini-circuits ZABDC20-322H); (6) circulator with an isolation of 25 dB, and; (7) two average power sensors (Telemakus TED8000-40) measuring incident and reflected power. In order to record any effects without appreciably heating the sample, this system was able to deliver pulsed input power of 26.5 dBm (0.45 W rms), which is considered sufficient to record a measurable response while minimizing the thermal effect.[29] It was also powerful enough to produce up to 32-W rms power to explore the response at much higher levels. To do this, a variable attenuator (4) was added to the circuit in order to vary the output power when needed. This required measuring the exact output power before each run using a broadband power sensor (8) (Rhode & Schwarz NRP-Z81). The microwave switch (2) enabled the delivery of power in controlled pulses rather than in a continuous manner in order to avoid heating the sample. We routinely controlled the average power delivered by changing the duty cycle, defined to be % of time during the regular pulsing that the microwave power is switched on. A vector network analyzer (VNA) (Keysight Technologies Fieldfox N9923A) was used to measure and record the reflected power via measurement of the voltage reflection coefficient S_{11}, of the cavity to achieve critical coupling of the cavity for maximum power delivery. A circulator (6) was used to protect the power amplifier from the reflected power from the cavity in case there is an unexpected mismatch.

2.4 *Software*

An in-house LabVIEW program was designed to control the microwave generator and simultaneously record the reflected power (via S_{11}) and power delivered to the cavity as the bacteria were subjected to microwave pulses. It also produced a resonant frequency sweep between each treatment. The photon counter (H7467, Hamamatsu) (9) was controlled using a separate LabVIEW program for data acquisition and processing using a 100-ms integration time for all the experiments as this is commensurate with the bacterial response times. This program was also used to plot photon emission rates as a function of time. Each Telemakus device was operated using its own driver, allowing full control over the microwave parameters (e.g., operating frequency and duty cycle). For data synchronization, it was possible to monitor the excitation times by multiplying the integration times by the integrated numbers and visually recording the start and end times for each excitation period. This method proved to be accurate enough for the reaction times that were observed.

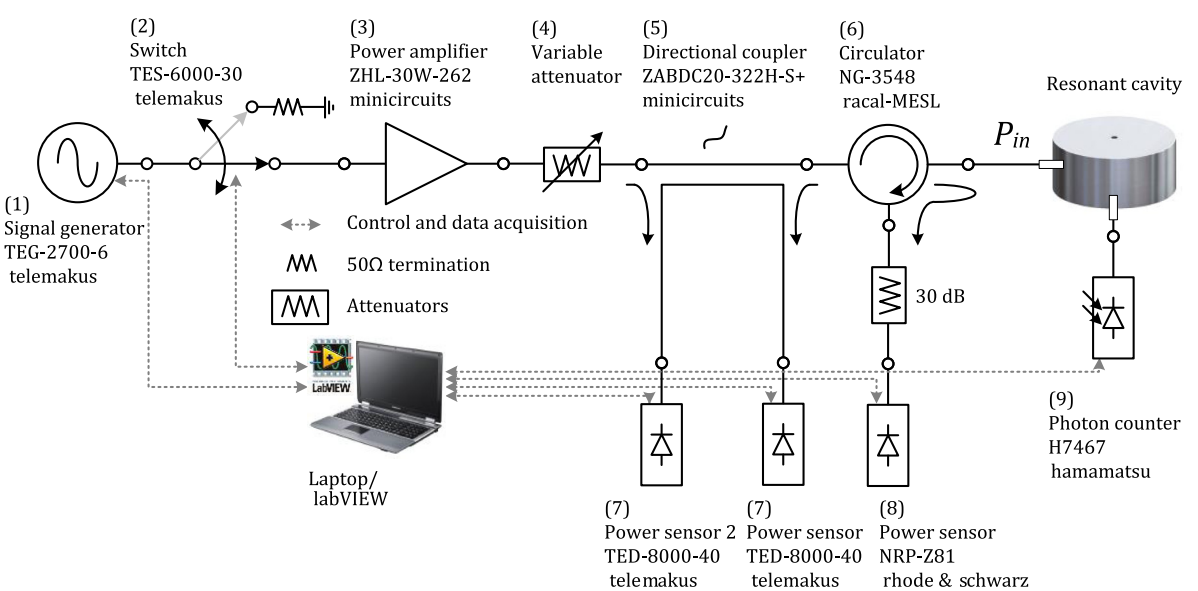

Fig. 2 Microwave circuitry and control system.

2.5 *Experimental Setup*

The aim of these experiments was to investigate the biological response of *V. fischeri* to the separate effects of electric and magnetic fields in the resonant cavity. In the TM_{010} mode, the peak E- and H-field regions are well-separated, and it was, therefore, possible to expose the cells to each field by carefully routing the Tygon sample tube (0.89-mm internal diameter). A precision peristaltic pump (ISMATEC Reglo digital) was used to feed the cell suspension into the cavity through the Tygon tube held in either of the fields within the cavity, and flow was stopped before irradiation. The sample tube was placed in the axial orientation for E-field excitation and circumferential orientation for H-field excitation. The total sample volume in both orientations was 47.4 μl. It was also used to flush the bacterial suspension between runs, thus presenting a new population (from an identical batch) for each run. For microwave H-field exposure at 2.45 GHz, bacterial suspensions were exposed to the maximum available power of 32 W rms and duty cycles of 10%, 20%, 40%, 50%, and 100%. For microwave E-field exposure at 2.45 GHz, bacterial suspensions were exposed to 0.45 or 4.5 W rms at duty cycles of 2%, 5%, and 10%. In all instances, the microwave pulse period was 100 ms and the "off" time varied according to the duty cycle required. The corresponding E- and H-field intensities at the axial circumferential positions are summarized in Table 1. The E and H fields have been calculated using finite-element modeling and these have been shown in our previous paper.[29] Such plots show the field distributions, but one still has to perform a calculation to determine the absolute value of the E field on axis, which can then be used to normalize all E- and H-field values at other positions. To do this, we equate the power in to the cavity to the power dissipated in the suspension, and in doing so we end up with the E-field normalizing factor used in Table 1. The specific absorption rate (SAR) for the E-field excitation is 4.5 W dissipated in a sample volume of 47.4 μl, which equates to 95 kW/kg. However, this is the peak SAR and, since we pulse our measurements, multiplication of this figure by the associated duty cycle is required to determine the time averaged SAR. Although the heat sinking arrangements are different for the axial and circumferential samples, this is of no issue for temperature rise since in the former arrangement there is negligible sample heating.

Table 1 Electric (E)- and magnetic (H)-field levels at 2.45 GHz averaged across the entire bacterial suspension within the TM_{010} mode cavity when the sample tube is placed separately in the axial or circumferential positions. The first the sample was tested in the E field (axial) and then a different sample, containing the same density and volume of bacteria in artificial seawater buffer, was tested in the H-field (circumferential) orientation, with critical coupling achieved for each measurement.

	E_z (V/m)	H_Φ (A/m)
Tube in axial position		
0.45 W rms	4240	5.15
4.5 W rms	13,400	16.3
Tube in circumferential position		
32 W rms	118	183

2.6 *Cavity Coupling*

All experiments described in this paper used the lowest resonant mode TM_{010} of the other higher order resonant modes which co-exist. Depending on the dielectric properties of the material placed within the cavity, the resonant frequency and Q factor of the cavity may be altered due to associated changes in the energy stored and energy dissipated, respectively. These changes are quantified by "perturbation theory," which is based on the assumption that the actual fields of a material-filled cavity are not greatly different from those of the unperturbed cavity.[35] A high Q means low losses, and vice versa. The Q factor of the sample-filled cavity is determined by the conductor losses in the cavity walls and the dielectric losses in the sample, the latter usually being dominant for aqueous samples. For the experiments presented here, Q factors were calculated from data collected using a VNA by measuring the reflected power S_{11} against frequency and subsequent curve fitting to obtain Q, resonant frequency, and coupling coefficient g to the cavity; this latter (dimensionless) quantity is defined via the input impedance of the cavity at resonance, which can be written $Z_{\text{in}} = gZ_0$, where Z_0 is the system impedance, in our case 50 Ω. Curve fitting to the measured $|S_{11}|$ in the frequency domain yields the loaded Q factor (Q_L, i.e., including the effects of the coupling structure), coupling coefficient g, and resonant frequency f_0. The unloaded Q factor (Q_U) is simply related to the loaded Q via $Q_U = (1+g)Q_L$, and this value is used to estimate the peak E and H fields within the cavity. All microwave connections are via coaxial lines of characteristic impedance 50 Ω. The actual coupling structure is a loop, which terminates a microwave *N* connector, which couples to the high H field of the TM_{010} mode close to its perimeter. The loop can be rotated, allowing fine adjustment of the coupling coefficient g. The cavity is said to be critically coupled when maximum power transfer between the resonator and the feedline is achieved ($|S_{11}| = 0$). This is when the device is impedance matched to the input circuitry at the resonant frequency, i.e., when $g = 1$. The goal is, therefore, to obtain a value of g as close to 1 as possible by fine initial adjustment of the orientation of the coupling loop, in order to ensure maximum power transfer to the cavity, and so to utilize effectively all of the microwave input power in generating high electromagnetic field amplitudes within the cavity. When critical coupling is attained, S_{11} tends to zero, giving a pronounced "dip (in dB scale)" when measured using the network analyzer. In practice, values of $|S_{11}|$ of <0.05 are achieved, giving a measured insertion loss of less than −25 dB at resonance.

2.7 *Photon Counting*

The photomultiplier of an integrated photon counting device (Hamamatsu H7467 series) was powered from a stabilized 5 V DC supply (Keysight Technologies) and optically coupled through a fiber-optic cable to the catheter tube containing the bacterial suspension delivered for microwave component field exposure (a selected volume of 47.4 ml of the pumped stream). This detector has a spectral response between 300 and 650 nm with a peak sensitivity wavelength of 420 nm that makes it ideal for its use with organisms exhibiting maximal bioluminescence at around 490 nm. The photomultiplier integration time was 100 ms. Due to its high sensitivity, it was essential to rigorously isolate the detector from any ambient light to avoid any light leaks and ensure that it was stored for at least 30 min in

total darkness before use in order to reduce background dark current to a minimum and signal-to-noise ratio to a maximum.

2.8 *Temperature Measurements*

An infrared thermal imaging camera (Micro-Epsilon thermoIMAGER TIM 640) was used to measure temperature changes during experiments. The camera was carefully focused on the sample tube through a side port in the cavity and is sensitive to within 1°C, has a range of −20°C to +900°C at ambient temperature (0°C to 50°C) and an acquisition rate of 30 ms. All temperature values quoted represent the maximum temperature measured across the sample (5 mm). Note that the temperature measurements overshoot the microwave excitation period due to the lag between the temperature of the cell suspension and that of the sample tube (the thermal imaging camera being focused on the outer surface of the latter).

3 Results

3.1 *Critical Coupling*

Resonant traces for S_{11} are shown in Fig. 3 and accompanying coupling parameters given in Table 2, for the E-field excitation configuration either with the cell suspension in artificial seawater or for an empty cavity. The high losses incurred when the seawater sample is present can be seen in Fig. 3(a). This affects the critical coupling condition as shown, so further adjustments of the coupling are required to ensure maximum power transfer. Also listed in the associated table are the resonant parameters of resonant frequency, Q factors, and coupling coefficient g, linked to the traces shown. Similar traces are shown in Fig. 3(b), this time for the H-field configuration. In this configuration, it is observed that the loss caused by the presence of the cell suspension is hardly detectable and a high Q factor is maintained, even when the aqueous sample is present. In either sample position, we do not plot the control data for a blank sea water sample as, within experimental error, the sea water trace is identical to that for a bacterial sample; this is to be expected, since the bacteria occupy a small volume fraction (<0.1%) and have dielectric properties close to sea water.

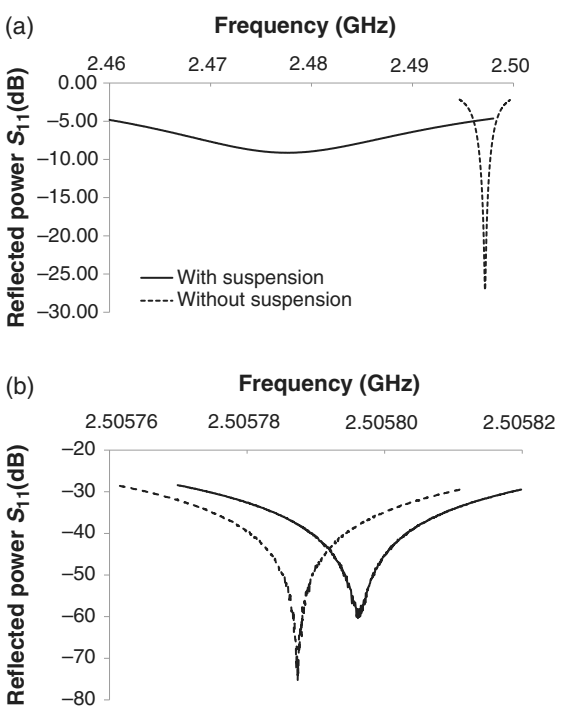

Fig. 3 (a) The magnitude of the cavity's amplitude reflection coefficient S_{11} in the frequency domain for the the E-field configuration and (b) H-field configuration, with (continuous trace) and without (dashed trace) cell suspension. Note the profound difference in frequency scale between (a) and (b).

Table 2 Calculated values for the loaded quality factor (Q_L), the coupling coefficient g, and unloaded quality factor (Q_U), together with the TM_{010} resonant frequency f_0, derived from the data presented in Figs. 3(a) and 3(b) for the E and H fields. All measurements were taken at low power (1 mW).

	f_0 (GHz)		Q_L		g		Q_U	
Field	E	H	E	H	E	H	E	H
Empty	2.5073	2.5073	1396	1396	0.975	0.975	2757	2757
With tube	2.4972	2.5058	919	1427	0.902	1.000	1747	2854
Tube + cells	2.4782	2.5058	37.2	1512	0.477	0.999	55.0	3021

3.2 *Background Bioluminescence*

We measure "dark" background photon counts, which are acceptably low, <4 photons/s obtained with 47.4 ml of artificial sea water in the absence of bacteria in the Tygon tube within the cavity. Similar results were obtained irrespective of whether the E- or H-field configurations were employed provided that the photomultiplier was always completely shielded from ambient light and the photocathode was stored and equilibrated under these conditions. It was also necessary to determine the decay of light emitted from the bacteria in their starved condition in seawater. Prior to microwave exposure, all bacterial samples are thermally equilibrated in the cavity for around 30 min. Typical microwave exposure occurs over a timescale of around 300 s. The time constant of the natural decay of bioluminescent light output is ∼2 days, so over a typical experiment there would be a natural decay of around 0.2%, which is negligible compared the effect of small thermal fluctuations (of the order of 0.1°C).

3.3 *Magnetic (H) Field Effects on Bacterial Bioluminescence*

V. fischeri cell suspensions were subjected to pulsed H field for 10 s (between $t = 10$ s and $t = 20$ s) as shown in Fig. 4. Different duty cycles were tested, ranging from 10% to 100% for an output power of 32 W rms, resulting in a maximal H-field strength of 183 A/m. In all cases, there was no noticeable variation in light emission during or after H-field excitation of the cells.

3.4 *Electric (E)-Field Effects on Bacterial Bioluminescence*

Light emission from suspensions of *V. fischeri* responded to microwave E-field pulses at all power levels and duty cycles

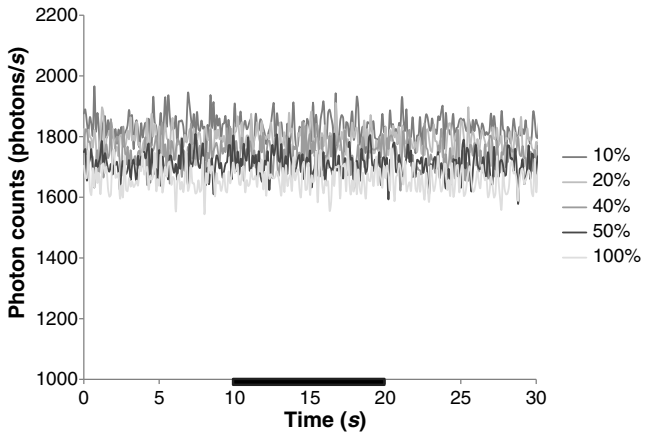

Fig. 4 The response of *Vibrio fischeri* light output to magnetic field excitation at 32 W rms and duty cycles of 10%, 20%, 40%, 50%, and 100%. The time duration of exposure is indicated by the black bars on the *x* axis. These traces are representative of at least two independent experiments.

tested. To investigate the sensitivity of bacterial bioluminescence to microwave E-field exposure and examine whether the effect is thermal or nonthermal in origin, simultaneous temperature measurements were conducted alongside photon counts over a range of duty cycles: 2% [Figs. 5(a) and 5(b)], 5% [Figs. 5(c) and 5(d)], and 10% [Figs. 5(e) and 5(f)], and at 0.45 W rms [Figs. 5(a), 5(c), and 5(e)] and 4.5 W rms [Figs. 5(b), 5(d), and 5(f)]. At 0.45 W rms, equivalent to an E-field intensity of 4.24 kV/m, temperature increases of 0.6°C, 1°C, and 1.5°C (at rates of 0.02, 0.03, and 0.05°C/s) were observed for duty cycles of 2%, 5%, and 10% [Figs. 5(a), 5(c), and 5(e)], respectively. This was accompanied by a 10% enhancement in light output for all three duty cycles tested, at increasing photon emission rates of 0.4, 0.6, and 0.7%/s, respectively, for each duty cycle. In the case of 10% duty cycle [Fig. 5(e)], this initial enhancement of bioluminescence was followed by suppression in light output between 16 and 30 s E-field exposures (a reduction of 10%). At the end of the 30-s treatment time, there was an immediate recovery in light output (15% enhancement) at a rate of 0.8%/s, after which a steady-state was achieved, and light output followed a natural decay curve (the latter also being the case for 2% and 5% duty cycle treatments).

At 10 times higher power (4.5 W rms, equivalent to 13.4 kV/m), temperature increases of 3.2, 5.4, and 6.3°C/s (at rates of 0.11, 0.18, and 0.21°C/s) were observed for duty cycles of 2%, 5%, and 10% [Figs. 5(b), 5(d), and 5(f)], respectively. In all cases, bacterial bioluminescence responded quickly (within the 100-ms acquisition time) and sensitively to the 100-ms microwave E-field pulses. At duty cycles of 2%, 5%, and 10%, the average rate of suppression in bacterial light output during every 100 ms E-field pulse was 0.57 ($\pm$0.31), 0.94 ($\pm$0.58), and 0.59 ($\pm$0.50)%/s, respectively. Note that the total excitation time was 30 s in all experiments, apart from that of 10% duty cycle, which was 15 s, due to the high degree of inhibition observed over this exposure time. There was no significant difference between the inhibition and recovery rates during or after the microwave E-field-pulses at all duty cycles tested. Likewise, there was no significant difference between the percentage changes in bioluminescence during these inhibitory and recovery phases, when all data was pooled together [Fig. 5(g)]. However, there was a general trend of increasing stimulatory and inhibitory rates from pulse 1 to 6, followed by a decrease in these rates from pulse 6 to 12, as light levels approached zero. Over the total exposure time, the overall rate of inhibition of bacterial bioluminescence was 3.1, 3.1, and 5.8%/s. The overall rate of recovery of bacterial bioluminescence following exposure was 6.1, 0.5, and 0.1%/s, respectively, with steady-state established at 80%, 40%, and 20% of maximum light output levels.

3.5 *Thermal Effects*

Temperature increases were measured in all experiments where bacteria were exposed to microwave E field. The rate of temperature increase was proportional to the amount of energy (i.e., power and duty cycle) delivered into the cell suspension. The maximum temperature achieved was 32.2°C ($\Delta T = 6.3$°C at 10% duty cycle, 4.5 W rms, 15 s), which caused a significant decrease in light output, down to 3% of the maximum (i.e., a 97% decrease). The minimum increase in temperature observed was 0.6°C (2% duty cycle, 0.45 W rms). All temperature measurements are recorded in Table 3 and Figs. 5(a)–5(f).

In order to examine if the microwave E-field-induced effects on bacterial light output were entirely thermal in origin, or if there may be an "added effect" induced by E-field exposure, a conventional heating control was conducted for comparison. Figure 6 shows the effect of water bath heating to 31°C on bacterial light output. The results can be compared directly to the bacterial suspension that was exposed to 4.5 W rms, 5% duty cycle for 30 s, as the same maximum temperature of 31°C was achieved ($\Delta T = 5.4$°C for E-field exposure and 5.8°C for conventional heating). Water bath heating led to a maximum inhibition in light output of 15%, and returned to the baseline level after heating. In contrast, E-field excitation resulted in reduction of light output to 4%, which recovered to only 40% after exposure. It should be noted, however, that the rate of heating for E-field excitation was ~4 times faster for E-field excitation (0.15°C/s) than was the case for conventional heating (0.04°C/s).

4 Discussion

These results demonstrate a sensitive and rapid method for discriminating between E- and H-field effects using a luminescent biosensor. These data provide a more detailed examination of the sensitivity of this bioluminescent system to microwave E-field excitation to those published by us previously.[29] In this previous publication, perturbation of light output from the same bioluminescent sensor, *Vibrio fischeri*, by the E (axial orientation) but not H (circumferential orientation) field, was first described.

Response of bacterial bioluminescence to each 100-ms pulse is rapid (within the 100-ms acquisition time) and sensitive, increasing proportionally with increasing power delivery into the sample. To speculate upon which stages in the molecular process which culminates in light production by *V. fischeri* could be affected by microwave E-field exposure, it is necessary to consider the contribution of both thermal and nonthermal effects. Bioluminescent light production by the marine bacterium *V. fischeri* consists of a complex of multistage enzyme-catalyzed cyclic reactions that precedes the photophysical process of excited state formation and subsequent photon release[26,36] (see Fig. 7). The pathways producing the necessary chemical reductants to drive the terminal events are completely elucidated. In these events, the enzyme (luciferase), classified as a

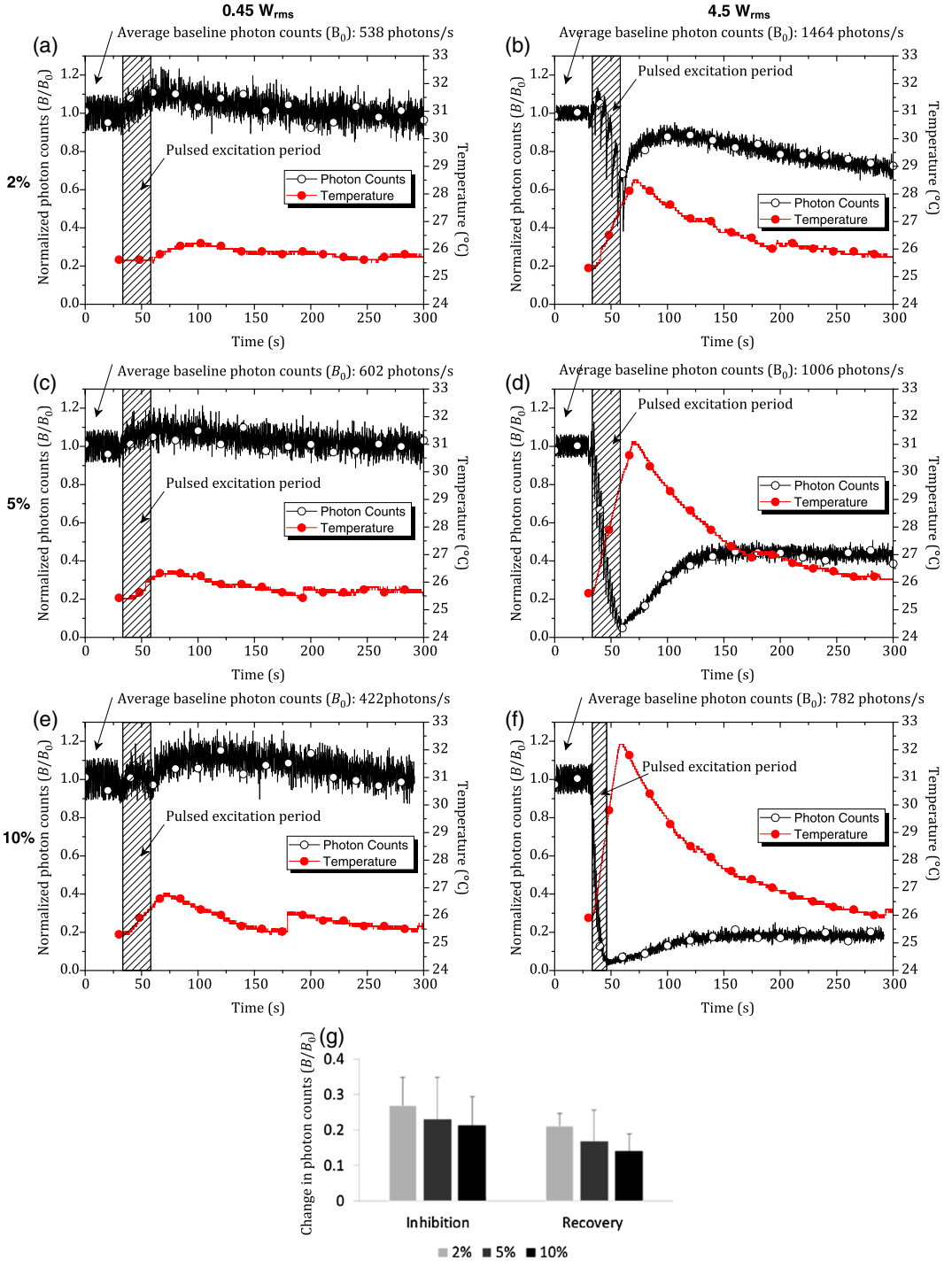

Fig. 5 (a) Simultaneous monitoring of *Vibrio fischeri* light output and temperature change under microwave E-field stimulation at 0.45 and 4.5 W rms and (a) and (b) 2%, (c) and (d) 5%, and (e) and (f) 10% duty cycle. The time duration of exposure is indicated by the shaded box. The exposure time for (a)–(e) was 30 s, and that of (f) was 15 s, due to the fact that microwave E-field excitation beyond this point resulted in complete inhibition of cells (i.e., no appreciable recovery of light emission). All experiments were repeated at least in duplicate. The *y* axis of (a)–(f) represents the photon counts (i.e., bacterial bioluminescence, *B*) normalized to the steady-state baseline level (B_0) before E-field exposure. The baseline photon counts before microwave exposure for each figure were as follows: (a) 538, (b) 1464, (c) 602, (d) 1006, (e) 422, and (f) 782 photons/s. (g) A summary of the change in light output achieved during the inhibitory and recovery phases during or immediately following E-field pulses at 4.5 W rms and 2%, 5%, and 10% duty cycles. The *y* axis of (g) represents the change in photon counts, based on data derived from (b), (d), and (f). Error bars represent the standard deviation, $n \geq 6$ successive pulses.

Table 3 A summary of the E-field (2.45 GHz) treatment regime, including the pulse period, recovery time, total exposure time, number of pulses, as well as the temperature elevations (temperature increase, ΔT and maximum temperature achieved, T_{max}) for 2%, 5%, and 10% duty cycle.

Duty cycle	Pulse period (ms)	Recovery time (s)	Total exposure time (s)	Number of pulses	ΔT, T_{max} (°C)
2		4.9	30	6	0.45 W = 0.6, 26.2
					4.5 W = 3.2, 28.5
5	100	1.9	30	15	0.45 W = 1, 26.4
					4.5 W = 5.4, 31.1
10		0.9	30 or 15[a]	30 or 15	0.45 W = 1.5, 26.8
					4.5 W = 6.3, 32.2

[a]4.5-W rms power only.

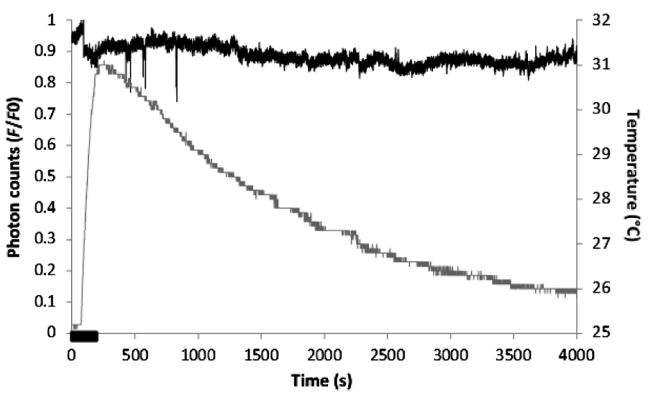

Fig. 6 Simultaneous monitoring of *Vibrio fischeri* light output and temperature change under conventional heating using a water bath. The time duration of heating is indicated by the black bar on the *x* axis.

flavin-dependent external mono-oxygenase, catalyzes the overall oxidation of reduced FMN ($FMNH_2$) and a medium-length chain aldehyde (e.g., dodecanaldehyde) to the corresponding carboxylic acid. In its reaction with O_2 (the third essential component of the reaction), the substrate (bacterial luciferin) gives a 4-a-flavin hydroperoxide on the benzenoid ring of the iso-alloxazine structure of the molecule and an equilibrium mixture of a hemiperoxyacetal and its peroxyhemiketal, formed by reaction with the aldehyde. The emitted photon in the bacterial strain employed here exhibits a spectral maximum output power at a free space wavelength of $\lambda_{max} \approx 490$ nm. The mechanism of formation of and photophysics of emission from the excited state of the flavin hydroperoxide is yet to be fully elucidated.[27,28] The chemiluminescent decomposition of flavin peroxyhemiacetal does not occur by charge-transfer initiation of chemoluminescence as formerly hypothesized (CIEEL),[27] but rather by the electron exchange-initiated luminescence (CTIL) for the thermolysis of a dioxetanone.[28] Furthermore, the luminophore of bacterial bioluminescence is now recognized as the first excited state of 4α-hydroxy-4a,5-dihydroxy FMN.[36] These terminal events (formation of the excited state and return to ground state) accompanied by photon release occur on ultrafast timescales of femtoseconds to nanoseconds.

The effects reported here do not initially perturb the slowest of these steps, as the biosynthetic ones [production of the autoinducer (AI), the transcriptional, and translational formation of the luciferase apoprotein] take tens of seconds to minutes. The formation of substrates of the bioluminescent system (biosynthesis of FMN and the long-chain aldehyde) during bacterial growth also involves moderately slow processes (timescales of 1 to 15 s). The metabolic pathways for the production of the coenzymes (ATP, NADH, and NADPH) also occur on timescales of the order of seconds. Thus these latter two classes of biochemical processes are possibly of interest in the elucidation of microwave E-field-mediated effects. The fast photophysical processes may be implicated but are too rapid to be studied in the experiments described here as data point collection was performed at a maximum acquisition rate of 100 ms.

The initial enhancement in light output at lower power levels could be due to the generation of free radical oxygen species ($HO^{\cdot}$, $O_2^{\cdot-}$, and/or $^1O_2$). Alternatively, free radical production might involve partial reduction of O_2 by direct interaction with microwave fields.[17] Extensive evidence has also been presented for downstream effects of plasma membrane voltage-gated calcium channel opening during exposure to electromagnetic fields in a variety of cells.[24,37–39] $NO^{\cdot}$ or peroxynitrite accumulates as a consequence of elevated intracellular Ca^{2+}, leading to beneficial or pathophysiological effects.[39,40] A voltage-gated Ca^{2+} channel has not been described in *V. fischeri*, but a structurally similar voltage-gated Na^+ channel has been described in *Bacillus halodurans*,[41] however, its function remains largely unexplored. Species of marine *Vibrio* possess channels (e.g., PomAB and MotXY) that are predicted to function as Na^+ channels,[42] which play an important part in driving the flagellar motor. However, their conductance has not been assessed.

Both the stimulation and inhibition of light output seen across the power levels and duty cycles tested could be due to E-field induced heating. The temperature optimum for the luciferase enzyme in *V. fischeri* is 25°C, with the enzyme becoming unstable above 30°C. Indeed, for duty cycles of 5% and 10% at 4.5 W rms, light output approaches zero when the temperature reaches 30°C. A step-wise increase in the rate of inhibition of bioluminescence is observed below 30°C at 2%, 5%, and 10% duty cycle under the same power level. Therefore, the changes in bacterial light output observed may be due to the linear rise in temperature observed and its direct effect on the stability of luciferase. At 10 times lower power (0.45 W rms), the enhancement in bioluminescence observed may also relate in temperature effects, with a slight elevation in temperature leading to an increased availability of the substrates required for bioluminescence.

5 Conclusions

Biological systems with intrinsic luminescent properties serve as powerful and noninvasive bioreporters for real-time and label-free monitoring of cell physiology.[43,44] In this context, bacterial bioluminescence has been used as a biosensor for determining the O_2 affinities of living cells[45] (sensitive to 10^{-8} MO_2) and for monitoring water toxicity.[46] This current work demonstrates the rapid response and sensitivity of *V. fischeri* light output as a noninvasive bioreporter of the effects of microwave E field. Developing a deeper understanding of the molecular

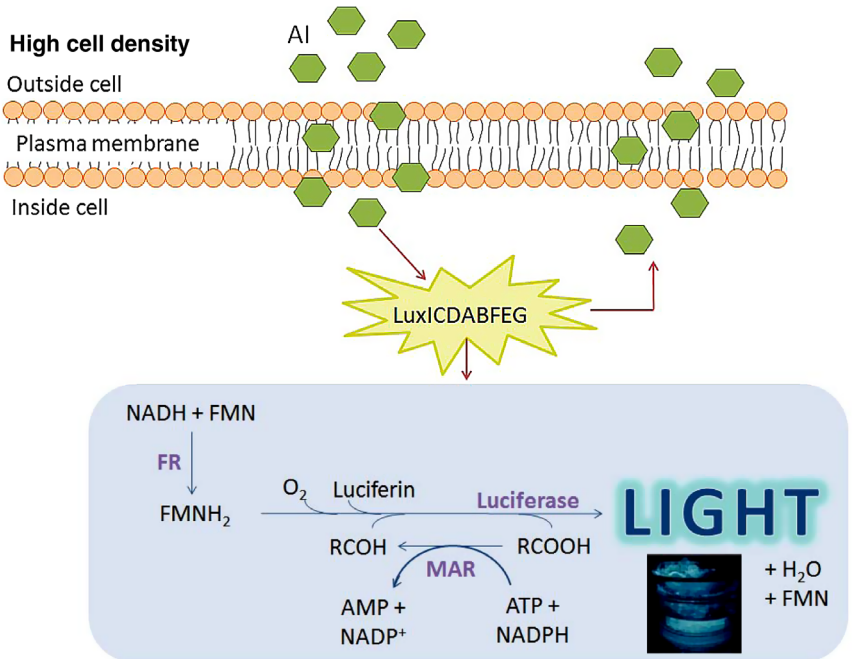

Fig. 7 A simplified schematic of the molecular basis of bioluminescence in *Vibrio fischeri*.[36] The AI presents only at high cell density, enters the cell, and activates the lux operon containing the luxCDABFEGH genes. These genes are transcribed and translated into all the proteins necessary to complete the bioluminescence reaction. Enzymes include flavin reductase, luciferase, and myristic acid reductase. Molecular dioxygen and the cofactors NADH and $FMNH_2$ are also required and are derived from bacterial metabolism, as well as ATP. A photon of blue-green light (490 nm) is released from the excited state of the flavin hydroperoxide photoemissive species as free energy.

mechanisms at play will enable a better appreciation of thermal and possible nonthermal microwave E-field-associated effects for dosimetry purposes.

Disclosures

The authors declare that they have no conflict of interest.

Acknowledgments

C. W. holds a Sêr Cymru II Fellowship part-funded by the European Regional Development Fund through the Welsh Government (TG/KJB/VSM:1063339). This work was also supported by a Sêr Cymru National Research Network in Advanced Engineering and Materials (NRN062) and ENSEIRB (Bordeaux, France). We thank Andrew Rankmore (School of Engineering, Cardiff University) for the mechanical construction of the microwave cavity. The *Vibrio fischeri* strain NRRLB-11177 used was kindly supplied by Dr. Michael H. Rayner-Brandes. Conceptualization: C. F. W., D. L., J. L., and A. P.; methodology: C. F. W., D. L., and A. P.; software: N. C.; investigation: C. F. W., G. M. G., N. C., and A. P.; formal analysis: C. F. W., G. M. G., and H. C.; writing: original draft, G. M. G., D. L., and C. F. W.; writing—review and editing: C. F. W., D. L., H. C., J. L., and A. P; funding acquisition: A. P., D. L., J. L., and C. F. W.; resources: A. P. and D. L.; and supervision: A. P., D. L., J. L, and C. F. W.

References

1. R. Baan et al., "Carcinogenicity of radiofrequency electromagnetic fields," *Lancet Oncol.* **12**(7), 624–626 (2011).
2. J. M. Samet et al., "Mobile phones and cancer next steps after the 2011 IARC review," *Epidemiology* **25**(1), 23–27 (2014).
3. T. Wu et al., "Safe for generations to come: considerations of safety for millimetre waves in wireless communications," *IEEE Microwave Mag.* **16**(2), 65–84 (2015).
4. L. Hardell, "World Health Organization radiation and health—a hard nut to crack," *Int. J. Oncol.* **51**(2), 405–413 (2017).
5. G. Coureau et al., "Mobile phone use and brain tumours in the CERENAT case-control study," *Occup. Environ. Med.* **71**(7), 514–522 (2014).
6. A. A. Warille et al., "Controversies on electromagnetic field exposure and the nervous systems of children," *Histol. Histopathol.* **31**(5), 461–468 (2016).
7. G. B. Dudley et al., "On the existence of and mechanism for microwave-specific reaction rate enhancement," *Chem. Sci.* **6**(4), 2144–2152 (2015).
8. S. S. Lin et al., "Microwave-assisted enzyme-catalyzed reactions in various solvent systems," *J. Am. Soc. Mass Spectrom.* **16**(4), 581–588 (2005).
9. C. Rougier et al., "Thermal and nonthermal effects of discontinuous microwave exposure (2.45 Gigahertz) on the cell membrane of Escherichia coli," *Appl. Environ. Microbiol.* **80**(16), 4832–4841 (2014).
10. I. Y. Belyaev et al., "Resonance effect of microwaves on the genome conformational state of E. coli cells," *Z. Naturforch. C* **47**(7–8), 621–627 (1992).
11. J. Miyakoshi, "Cellular and molecular responses to radio-frequency electromagnetic fields," *Proc. IEEE* **101**(6), 1494–1502 (2013).
12. L. Gherardini et al., "Searching for the perfect wave: the effect of radiofrequency electromagnetic fields on cells," *Int. J. Mol. Sci.* **15**(4), 5366–5387 (2014).
13. K. R. Foster et al., "Thermal response of human skin to microwave energy: a critical review," *Health Phys.* **111**(6), 528–541 (2016).
14. W. J. Zhi et al., "Recent advances in the effects of microwave radiation on brains," *Mil. Med. Res.* **4**, 29 (2017).
15. N. Halgamuge, "Critical time delay of the pineal melatonin rhythm in humans due to weak electromagnetic exposure," *Indian J. Biochem. Biophys.* **50**(4), 259–265 (2013).
16. M. Yang et al., "Mobile phone use and glioma risk: a systematic review and meta-analysis," *PLoS One* **12**(5), e0175136 (2017).

17. I. Belyaev, "Biophysical mechanisms for non-thermal microwave effects," in *Electromagnetic Fields in Biology and Medicine*, M. S. Markov, Ed., pp. 49–68, CRC Press, Boca Raton (2015).
18. F. E. Yates, "Ultradian rhythms as the dynamic signature of life," in *Ultradian Rhythms from Molecules to Mind*, D. Lloyd and E. L. Rossi, Eds., pp. 249–260, Springer, Berlin (2008).
19. M. A. Aon et al., "Chaos in biochemistry and physiology," in *Encyclopaedia of Biochemistry and Molecular Medicine: Systems Biology*, R. A. Meyers, Ed., pp. 239–276, 2nd edn., Wiley-VCH Verlag, Weinheim (2011).
20. A. L. Lloyd and D. Lloyd, "Chaos: its significance and detection in biology," *Biol. Rhythm Res.* **26**(2), 233–252 (1995).
21. H. Fröhlich, "Long-range coherence and energy storage in biological systems," *Int. J. Quantum Chem.* **2**(5), 641–649 (1968).
22. A. R. Vasconcellos et al., "Fröhlich condensate: emergence of synergetic dissipative structures in information processing biological and condensed matter systems," *Information* **3**(4), 601–620 (2012).
23. A. F. Fonseca et al., "Informational-statistical thermodynamics of a complex system," *J. Chem. Phys.* **112**(9), 3967–3979 (2000).
24. M. L. Pall, "Scientific evidence contradicts findings and assumptions of Canadian Safety Panel 6: microwaves act through voltage-gated calcium channel activation to induce biological impacts at non-thermal levels, supporting a paradigm shift for microwave/lower frequency electromagnetic fields action," *Rev. Environ. Health* **30**(2), 99–116 (2015).
25. D. Lloyd, "Flow cytometry, a technique waiting for microbiologists," in *Flow Cytometry in Microbiology*, D. Lloyd, Ed., pp. 1–9, Springer, Berlin (1993).
26. J. W. Eckstein et al., "Mechanism of bacterial bioluminescence: 4a,5-dihydroflavin analogs as models for luciferase hydroperoxide intermediates and the effect of substituents at the 8-position of flavin on luciferase kinetics," *Biochemistry* **32**, 404–411 (1993).
27. F. McCapra, "Mechanisms in chemiluminescence and bioluminescence —unfinished business," in *Bioluminescence and Chemiluminescence: Molecular Reporting with Photons*, J. W. Hastings, I. J. Kricka, and P. E. Stanley, Eds., pp. 7–15, John Wiley & Sons, Chichester (1996).
28. C. Hou et al., "Understanding bacterial bioluminescence: a theoretical study of the entire process, from reduced flavin to light emission," *Chemistry* **20**(26), 7979–7986 (2014).
29. C. F. Williams et al., "The separated electric and magnetic field responses of luminescent bacteria exposed to pulsed microwave irradiation," *Appl. Phys. Lett.* **109**(9), 093701 (2016).
30. D. Slocombe et al., "Microwave properties of nanodiamond particles," *Appl. Phys. Lett.* **102**, 244102 (2013).
31. J. A. Cuenca et al., "Study of the magnetite to maghemite transition using microwave permittivity and permeability measurements," *J. Phys. Condens. Matter* **28**, 106002 (2016).
32. D. M. Pozar, *Microwave Engineering*, pp. 272–316, 2nd edn., John Wiley and Sons Inc., New Jersey (1998).
33. M. Mehdizadeh, "Microwave/RF applicators and probes for material heating and plasma generation," 2nd ed., pp. 440, William Andrew, Elsevier Inc., Norwich, New York (2015).
34. D. T. Pooley et al. "Biological effects of millimetre-wave radiation: a high throughput screening system," *Rev. Sci. Inst.* **74**(3), 1296–1302 (2003).
35. S. Scheerer et al., "Bioluminescence of Vibrio fischeri in continuous culture: optimal conditions for stability and intensity of photoemission," *J. Microbiol. Methods* **67**(2), 321–329 (2006).
36. T. Miyashiro and E. G. Ruby, "Shedding light on bioluminescence regulation in Vibrio fischeri," *Mol. Biol.* **84**(5), 795–806 (2012).
37. J. Walleczek, "Electromagnetic field effects on cells of the immune system: the role of calcium signaling," *FASEB J.* **6**(13), 3177–3185 (1992).
38. D. J. Panagopoulos et al., "A mechanism for action of oscillating electric fields on cells," *Biochem. Biophys. Res. Commun.* **272**(3), 634–640 (2000).
39. W. R. Adey, "Biological effects of electromagnetic fields," *J. Cell Biochem.* **51**(4), 410–416 (1993).
40. D. J. Panagopoulos, "Mobile telephony EMFs effects on insect ovarian cells. The necessity for real exposures bioactivity assessment. The key role of polarization, and the ion forced-oscillation mechanism," in *Microwave Effects on DNA and Proteins*, C. D. Geddes, Ed., pp. 1–48, Springer, Berlin (2017).
41. R. Koishi et al., "A superfamily of voltage-gated sodium channels in bacteria," *J. Biol. Chem.* **279**(10), 9532–9538 (2004).
42. T. Yorimitsu and M. Homma, "Na^+-driven flagellar motor of Vibrio," *Biochim. Biophys. Acta Bioenerg.* **1505**(1), 82–93 (2001).
43. M. Cifra and P. Pospíšil, "Ultra-weak photon emission from biological samples: definition, mechanisms, properties, detection and applications," *J. Photochem. Photobiol. B* **139**, 2–10 (2014).
44. M. Cifra et al., "Endogenous biological chemiluminescence for probing oxidative effects of electric pulses," [abstract] BioEM2018, Piran, Portorož, Slovenia (2018).
45. R. Oshino et al., "A sensitive bacterial luminescence probe for O_2 in biochemical systems," *Biochem. Biophys. Acta* **273**(1), 5–17 (1972).
46. D. T. Pooley et al., "Continuous culture of photobacterium," *Biosens. Bioelectron.* **19**(11), 1457–1463 (2004).

Catrin F. Williams received her BSc degree (honours) and PhD both in microbiology from Cardiff University School of Biosciences (BIOSI). She currently holds a Sêr Cymru II fellowship at ENGIN, which investigates the biological effects of microwave fields. In 2017, she was named as one of the top 50 women in engineering (Women's Engineering Society and Telegraph) and 35 under 35 young business and professional women in Wales.

Gilles M. Geroni received his master's degree in electrical and electronic engineering from Cardiff University. During his time at Cardiff University, he investigated the real-time nonthermal effects of pulsed microwaves on living cells. He is now an electrical engineer consultant in building services.

David Lloyd received his BSc (honours) and his DSc degrees from Sheffield University in biochemistry, and his PhD from the University of Wales before joining the Biophysics Department at the University of Pennsylvania. He is now the honorary professor of microbiology at Cardiff University and HC Andersen professor at the University of Southern Denmark, with more than 50 years of experience of the application of minimally invasive techniques to microorganisms and mammalian cells.

Heungjae Choi received his BSc, MSc, and PhD degrees from Chonbuk National University, Jeonju, Republic of Korea. He is currently a Sêr Cymru II research fellow working toward the commercialization of the microwave noninvasive blood glucose monitoring sensor at the Centre for High Frequency Engineering, Cardiff University, Cardiff, Wales, UK. His research interests include design of linear high-efficiency power amplifier, microwave noninvasive material characterization and sensing, and its healthcare application.

Nicholas Clark received his BEng (honours) degree in computer systems engineering and his PhD in microwave engineering from Cardiff University, UK. His research involved the application of microwave resonant structures and his specific interests include the characterization and heating of metal powders and structures and the development of precision microwave heating systems. He currently works as a control and analysis engineer for YASA Ltd. based in Oxford, UK.

Antoine Pirog received his BSc (honours) degree from Bordeaux University, France, and his MEng degree in electronics from ENSEIRB-MATMECA (Bordeaux Engineering School). His participation in the Cluster TIC Santé Aquitain led him to a specialization in medical applications of electronic devices. He is currently a PhD student in Bordeaux IMS Laboratory where he works on an innovative hybrid biosensor that extracts insulin secretion levels based on the electrical activity of pancreatic cells, monitored on microelectrode arrays.

Jonathan Lees is a senior lecturer at Cardiff University, with research focusing on the design and optimization of high power, high-efficiency radio-frequency power amplifiers (RFPAs). His work includes the first published Gallium Nitride Doherty amplifier for mobile communications applications and more recently RFPAs for medical diagnostic and domestic heating applications. He recently won the Cardiff

University Business Innovation award, 2017, for his work developing autonomous weighing solutions.

Adrian Porch is the research leader of Cardiff's Centre for High Frequency Engineering. He has 30 years of research experience in the fundamental properties, electromagnetic modeling, and applications of materials at microwave frequencies. He is a champion of interdisciplinary research, stemming from his first degree in natural sciences (Cambridge University, 1983 to 1986) and his PhD from Cambridge's IRC in superconductivity (1986 to 1989). In recent years, his research has expanded into the area of medical microwave devices.